nature chemistry

Article https://doi.org/10.1038/s41557-023-01158-5

Autonomous and directional flow of water and transport of particles across a subliming dynamic crystal surface

In the format provided by the authors and unedited

Supporting Information

Autonomous and Directional Flow of Water and Transport of Particles across a Subliming Dynamic Crystal Surface

Contents

Supplementary Notes

Supplementary Note 1. The hexachlorobenzene (HCB) surface is exceptionally complex and a model containing as many variables as HCB has not been studied previously. More specifically, the surface of HCB contains tapered, open, non-uniform, dynamic subliming channels that use water condensed from aerial humidity. In the related literature, there are several studies that use idealized surfaces to describe the movement of water in (1) tapered closed tubes, (2) open irregular channels or (3) aerial humidity, but none that incorporates all of the variables. For example, one study that details the effects on capillary rise in corners[1] used the following expression to determine the height water in relation to time:

$$\frac{h(t)}{a} \approx \left(\frac{\gamma t}{\eta a}\right)^{1/3}$$

where γ and η stand for the surface tension and viscosity of the liquid while $a = (\gamma/\rho g)^{1/2}$ is the capillary length, based on the liquid density ρ and gravity g. This equation express how fluid will rise along a corner at a rate of $h(t) \sim t^{1/3}$. However, this expression was derived from an experiment that utilizes a liquid reservoir and a static non-tapered channel against gravity which is different from our dynamic, tapered humidity driven surface that does not flow against gravity. Therefore, we conclude that the experimental conditions are not identical and this expression cannot be applied to our experiments.

A separate study that describes drop propulsion in closed tapered tubes[2] shows that the drops will spontaneous move towards a tapered end against gravity using the expression:

$$z_0 \approx \kappa^{-1}\left(\frac{2}{\alpha sin\theta}\right)^{1/2}$$

where z_0 is the equilibrium position of the drop, $\kappa^{-1} = \gamma/\rho g$, ($\gamma =$ surface tension, $\rho =$ density, g = gravity), a is the slope of tapered tube in degrees, and θ is the tilt of tapered tube in degrees. The expression is useful for showing how a droplet will move against gravity towards a tapered tube and finding the equilibrium position of a liquid plug inside of a conical tube. However the study is different from the HCB study in that the expression is used for closed tubes instead of the open channels found on HCB.

When discussing flow in open channels the most applicable expression to describe the flow rate is the Washburn equation which is:

$$x^2 = \gamma R \frac{cos\theta}{2\mu} t$$

where x is the position, γ is the surface tensions, R is the capillary radius, θ is the contact angle, μ is the viscosity, and t is the time. The work from Rye, Yost and O'Toole[3] showed that the Washburn behavior of $x^2 \sim t$ is obtained for all capillary surfaces' groves regardless of groove shape. When compared to the data obtained during the HCB experiments (Supplementary Figure 2) we can see the position has a linear correlation with time instead of $x^2 \sim t$ relationship so it does not follow the expected Washburn equation.

This deviation from the Washburn behavior however is expected because the water deposited on HCB is relative to the humidity in the air. Indeed, the experiment does not use a reservoir and it has been shown that the Washburn behavior is not obeyed during drying conditions[4]. Altogether, the previous literature has yet to describe a surface as complex as the dynamic surface of HCB.

However, we note that similar work investigating the surface tension transport of water by shorebird beaks describe the flow of water towards an apex of a wedge.[5] Granted the paper simulates a bird's beak by placing two plates in a "V" shape with varying degrees of increasing and decreasing the angle, the results from this work are useful for describing the Laplace pressure gradient caused by the two menisci of different sizes at opposite sides of a wedge as:

$$\text{Laplace pressure difference} = \frac{\gamma}{ax} - \frac{\gamma}{a(x+L)}$$

The authors go on to show that as the water approaches the apex, $x \ll L$ then the pressure difference between the menisci becomes $\gamma/(\alpha x)$, which corresponds to a pressure gradient of $\gamma/(\alpha x L)$. Calculation of the Laplace pressure difference water inside a wedge requires information on the size of the menisci at both ends. Since the menisci at two ends have not been observed in our study, we are unable to calculate the Laplace pressure difference.

Very recently, a paper was published showing how the surface of a *Sarracenia* trichome[6] uses hierarchical microchannels to transport water quickly. The trichome has rows of ribs that form channels and those channels gradually narrow towards the base to create a gradient in capillary force from the tip to the base. The mechanism is similar to what is proposed for HCB in our work as both contain open, narrowing channels though the *Sarracenia* trichrome channels narrow over its length, whereas the HCB channels narrow and widen over time. The authors of this latter article noted that although the trichome needle shape generates a Laplace pressure difference, the dominant driving force is hierarchical microchannel-induced capillary forces. Considering the similarities between the two surfaces, we believe a very similar phenomenon occurs in HCB.

Supplementary References

1. Ponomarenko, A., Quéré, D. & Clanet, C. A universal law for capillary rise in corners. *J. Fluid Mech.* **666**, 146–154 (2011).

2. Renvoisé, P., Bush, J. W. M., Prakash, M., & Quéré, D. Drop propulsion in tapered tubes. *EPL* **86**, 64003 (2009).

3. Rye, R. R., Yost, F. G. & O'Toole E. J. Capillary flow in irregular surface grooves. *Langmuir* **14**, 3937–3943 (1998).

4. Lade, R. K., Jochem, K. S., Macosko, C. W. & Francis, L. F. Capillary coatings: flow and drying dynamics in open microchannels. *Langmuir* **34**, 7624–7639 (2018).

5. Prakash, M., Quéré, D. & Bush, J. W. M. Surface tension transport of prey by feeding shorebirds: the capillary ratchet. *Science* **320**, 931–934 (2008).

6. Chen, H. et al. Ultrafast water harvesting and transport in hierarchical microchannels. *Nat. Mater.* **17**, 935–942 (2018).

Supplementary Figures

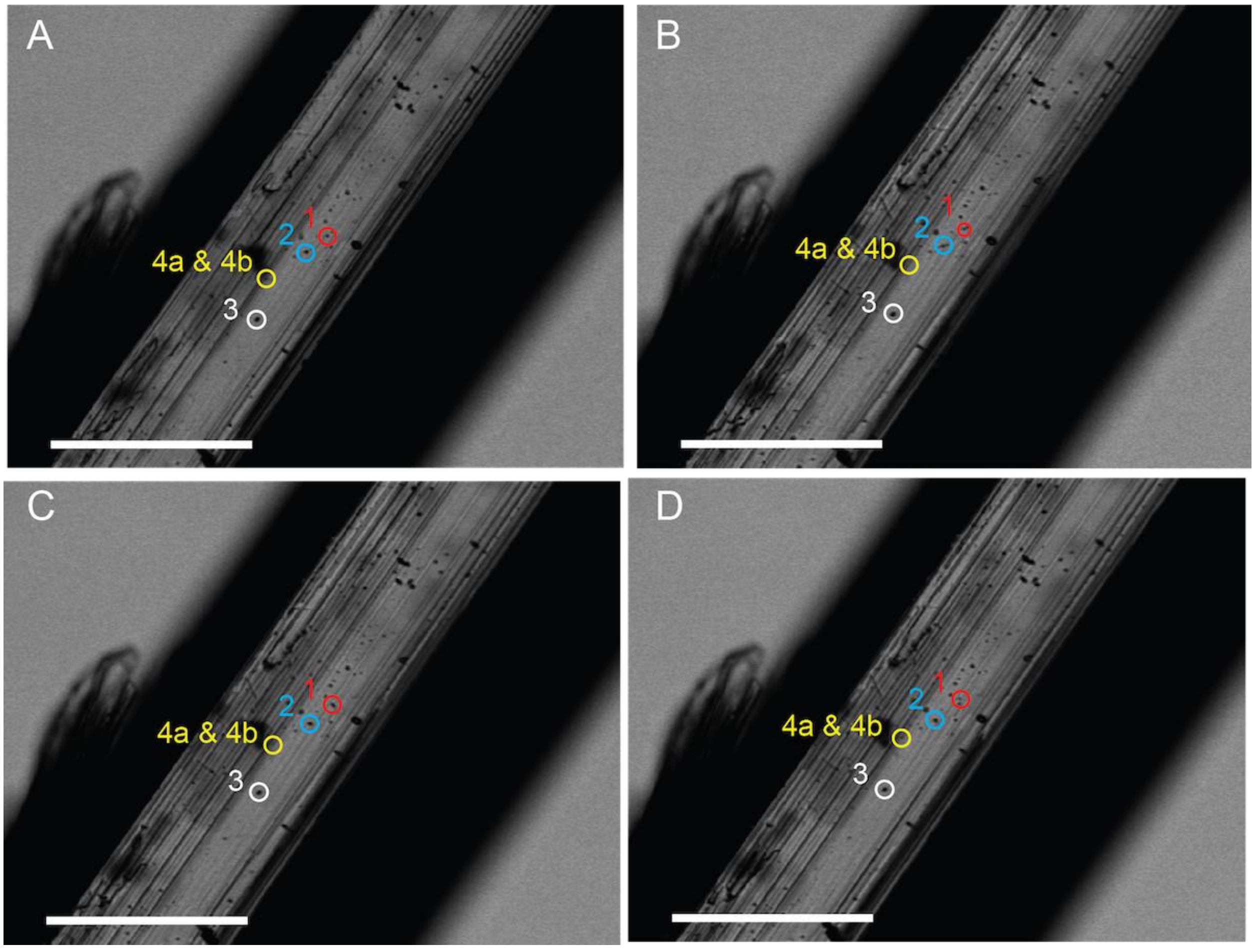

Supplementary Fig. 1. Confocal microscopic images of dust moving over the (001) surface of an HCB crystal for 670 min. (A) *t* = 0 min, (B) *t* = 220 min, (C) *t* = 440 min, (D) *t* = 670 min. The images show five particles autonomously moving along the channels of HCB. Scale bar in all panels = 100 μm.

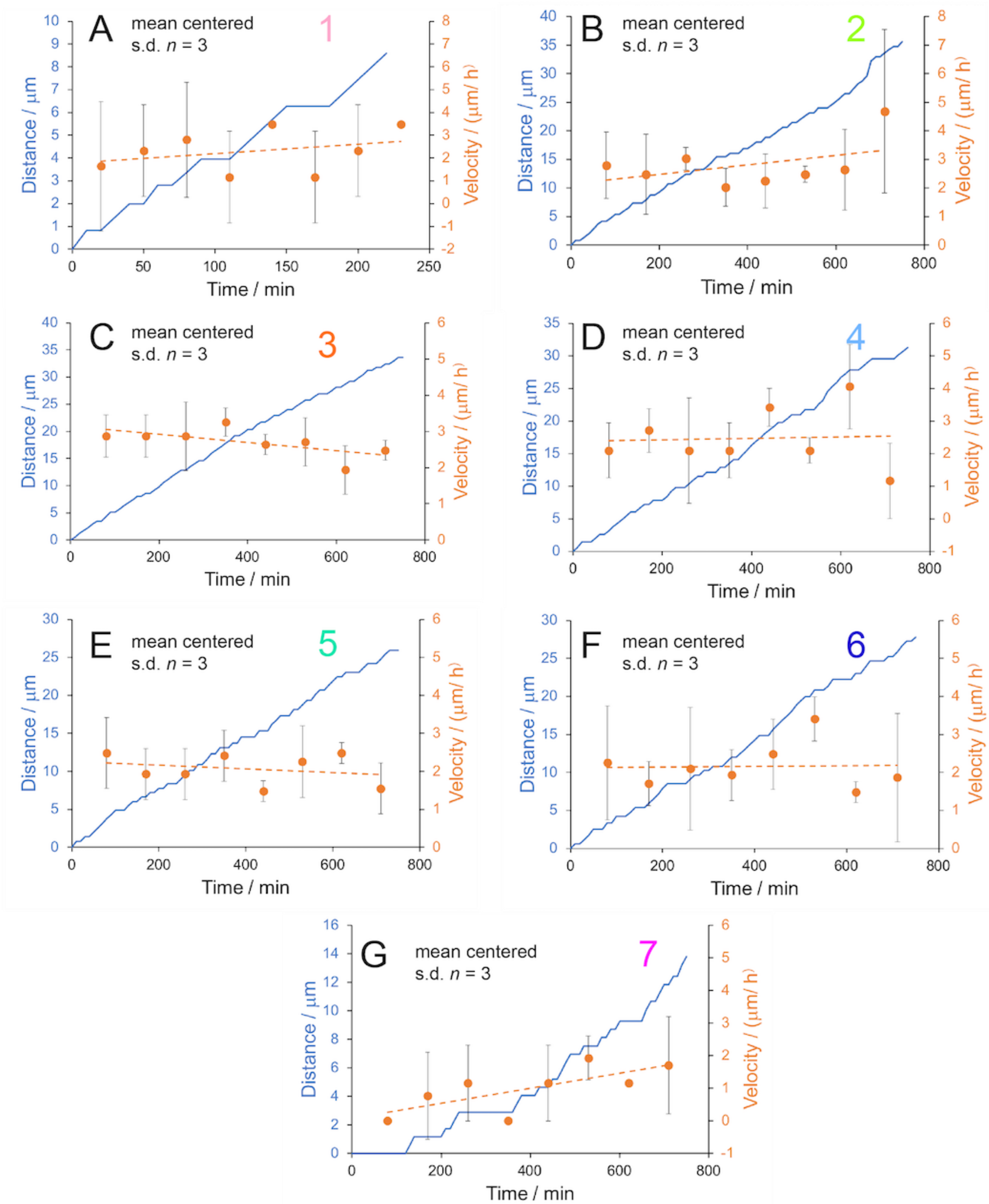

Supplementary Fig. 2. Movement of AgMPs at 21 ºC. The distance and velocity profiles of the tracked silver microparticles (AgMPs), labeled 1 – 7, during the optical observation at room temperature and 55% relative humidity. The velocity profiles show the particles move at fairly similar consistent rates at constant temperature and humidity, indicating a constant thermodynamic force such as sublimation was propelling them. The tracking of the particle labeled 1 ends at 220 min because the particle was stationary after this point.

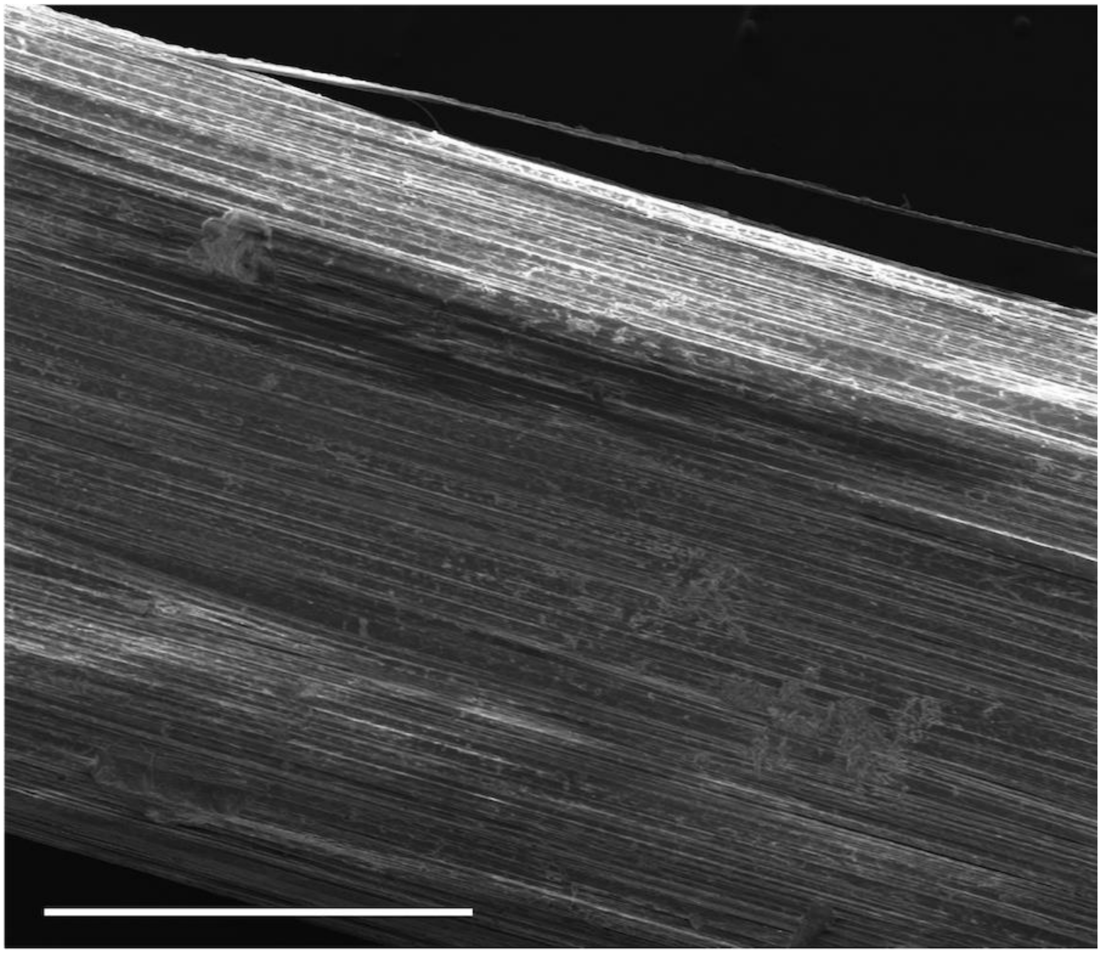

Supplementary Fig. 3. Scanning electron micrograph of the (001) face of an HCB crystal. The surface has many channels running along the [010] direction of similar but not identical width. Scale bar = 200 μm.

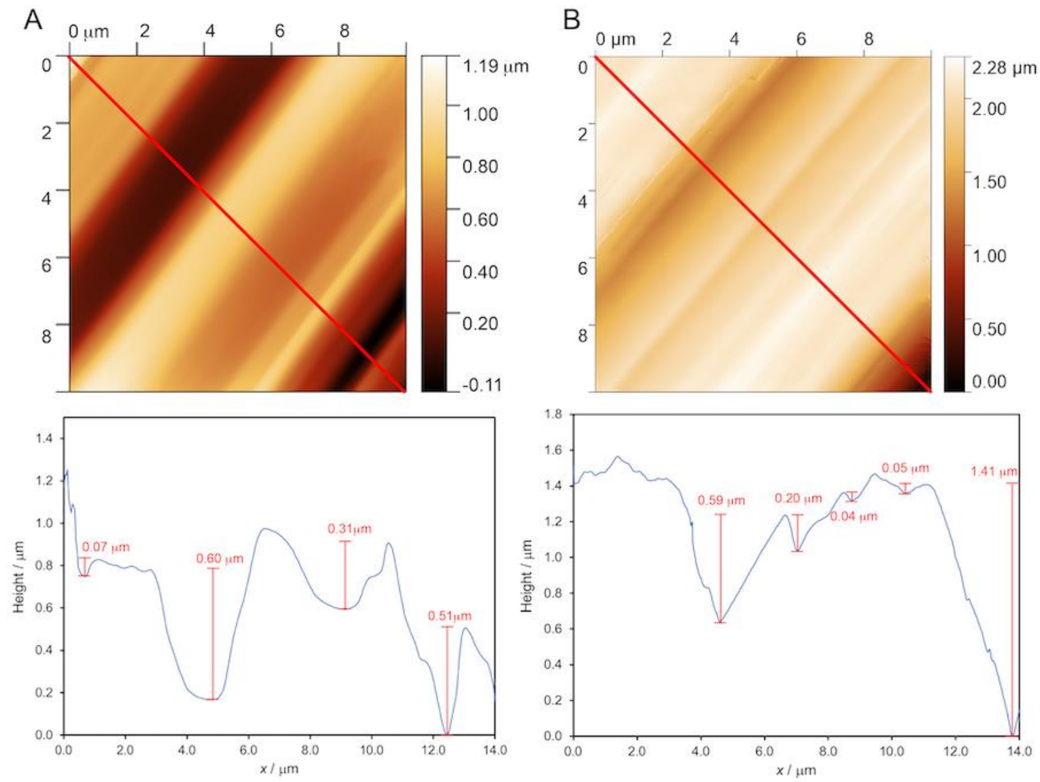

Supplementary Fig 4. AFM images of the HCB surface. AFM images and the corresponding height profiles of two HCB crystals used to measure the depth of the channels (one shown in panel A and one in panel B). The depth of the channels are shown in red.

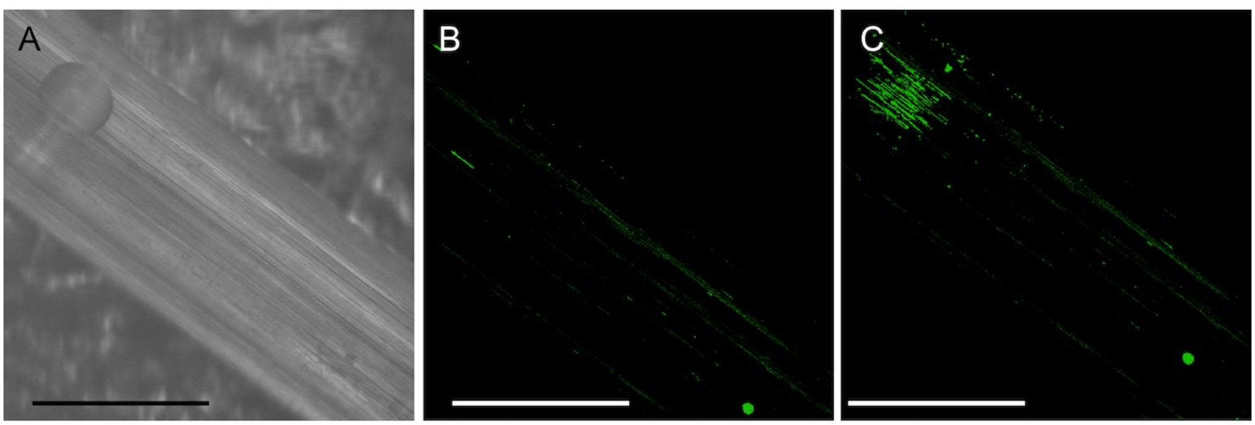

Supplementary Fig 5. A fluorescent dye dropcast onto an HCB crystal. (A) Optical image of a droplet of water containing 1% (mass/mass) Rhodamine B on an HCB crystal. (B,C) Confocal fluorescence image of the crystal before (B) and after the Rhodamine-B-dyed water was placed on its surface (C). The water droplet was spread preferentially along the channels and the fluorescent dye highlights the water moved in the [010] direction. Scale bar in all panels = 500 μm.

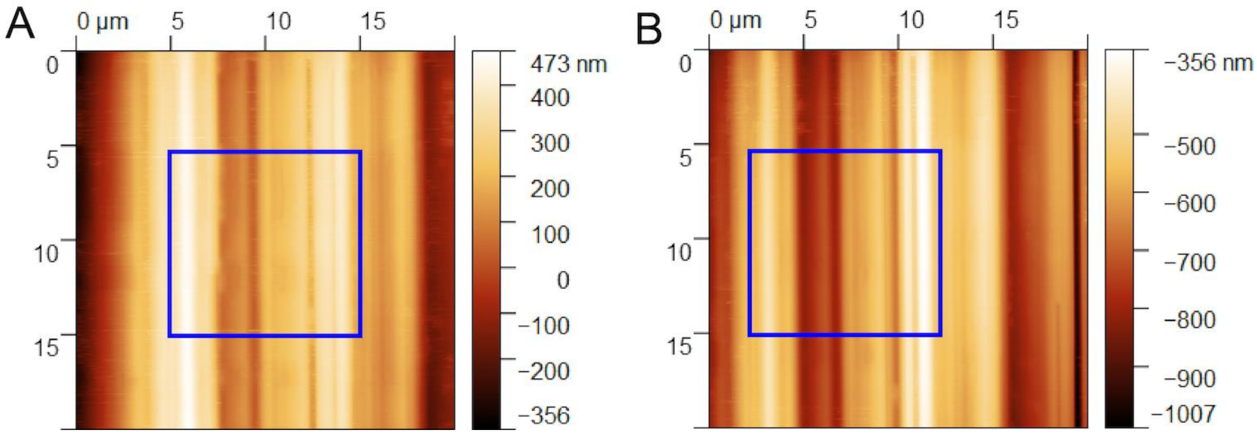

Supplementary Fig. 6. Testing the effects of an AFM tip on the imaged surface for prolonged scans. The AFM images were recorded at t = 0 h (A) and at t = 48 h (B). A 20 × 20 µm surface was initially imaged. A 10 × 10 µm area was then imaged for 48 h, and after 48 h the original 20 × 20 µm surface was imaged again. The blue box indicates the 10 × 10 µm area that was scanned for 48 h. Although the height of the sample decreased because the surface sublimed, no etching was found to occur on the scanned area. Moreover, thermal drift caused the scanned area to shift slightly to the left during the 48 h acquisition.

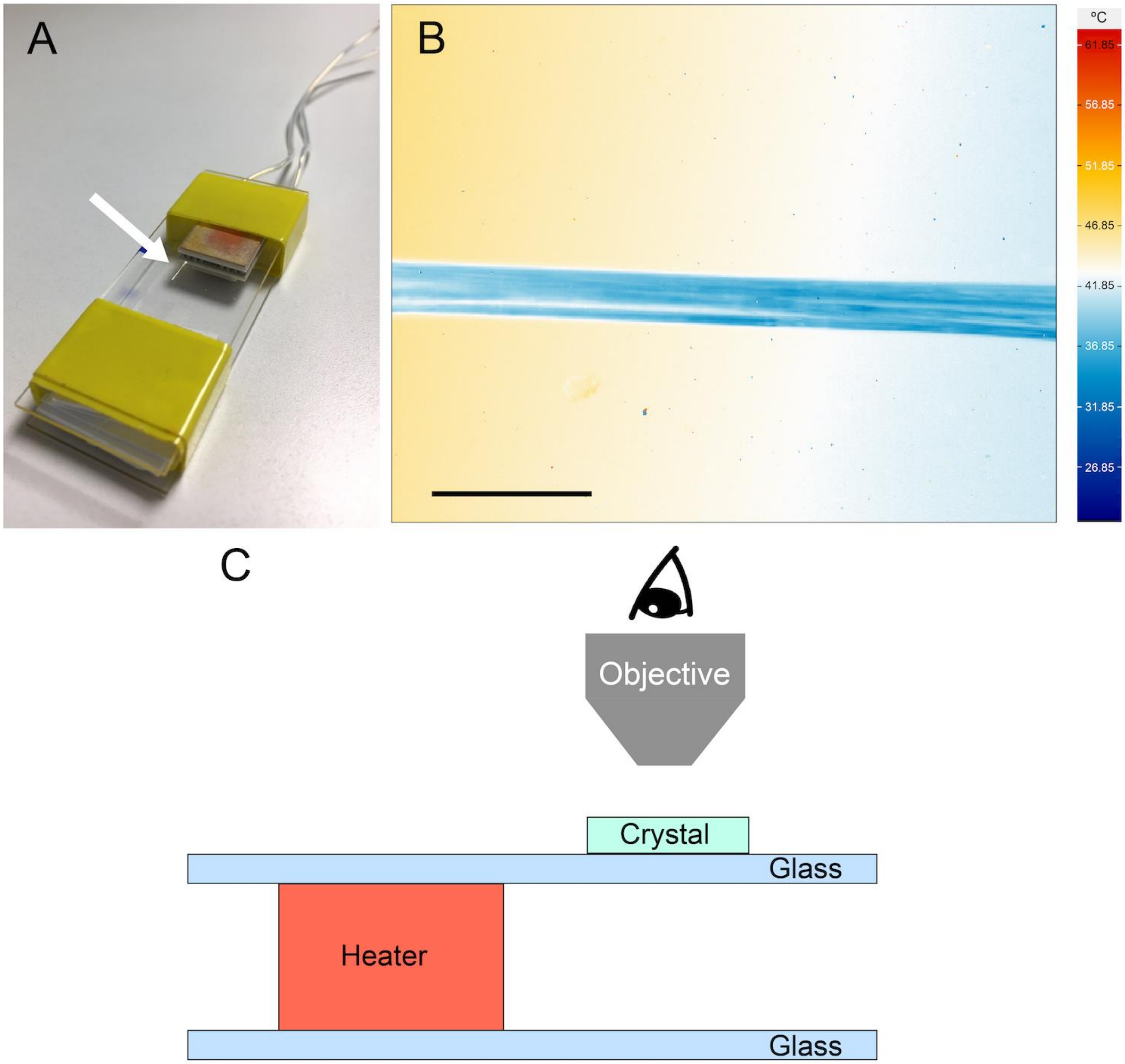

Supplementary Fig. 7. Heating apparatus used to apply non-uniform heating to an HCB crystal. (A) An optical image of a non-uniform heating stage with a crystal on it. A white arrow points to the crystal. (B) A thermal image of the stage with a crystal on it showing color-coded temperature range of 41.7–46.6 ºC across the heated stage and 34.7–41.5 ºC across the crystal. Scale bar = 1 mm (C) A schematic of the experimental setup.

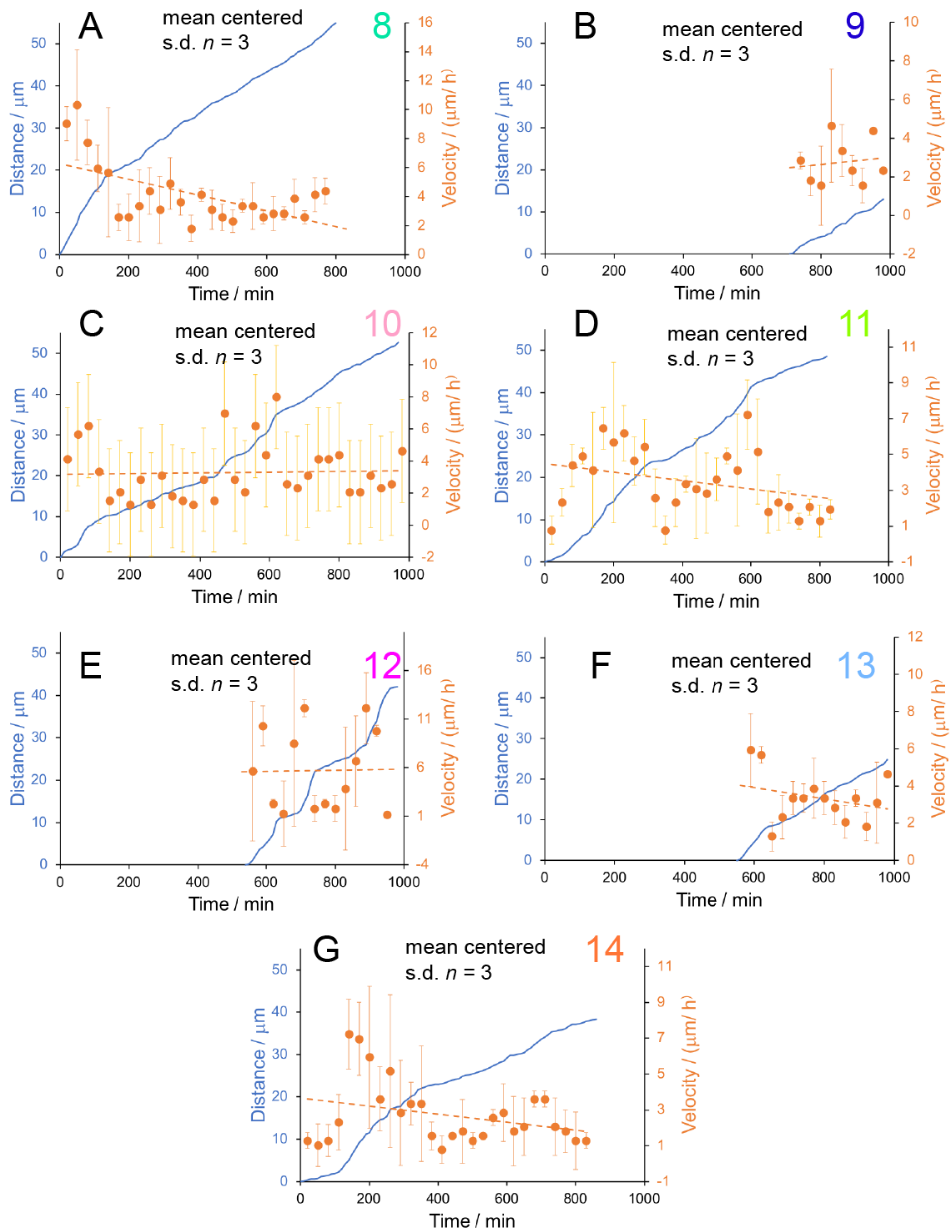

Supplementary Fig. 8. Movement of AgMPs at 34.7–41.5 ºC at 55% relative humidity. Distance and velocity profiles of the tracked particles during heating. The velocity profiles show the particles move at unpredictable and inconsistent rates at elevated temperatures, which is caused by the channels subliming and the particles exiting their controlled linear paths. Some particles start at non-zero times because they did not move when the experiment first began.

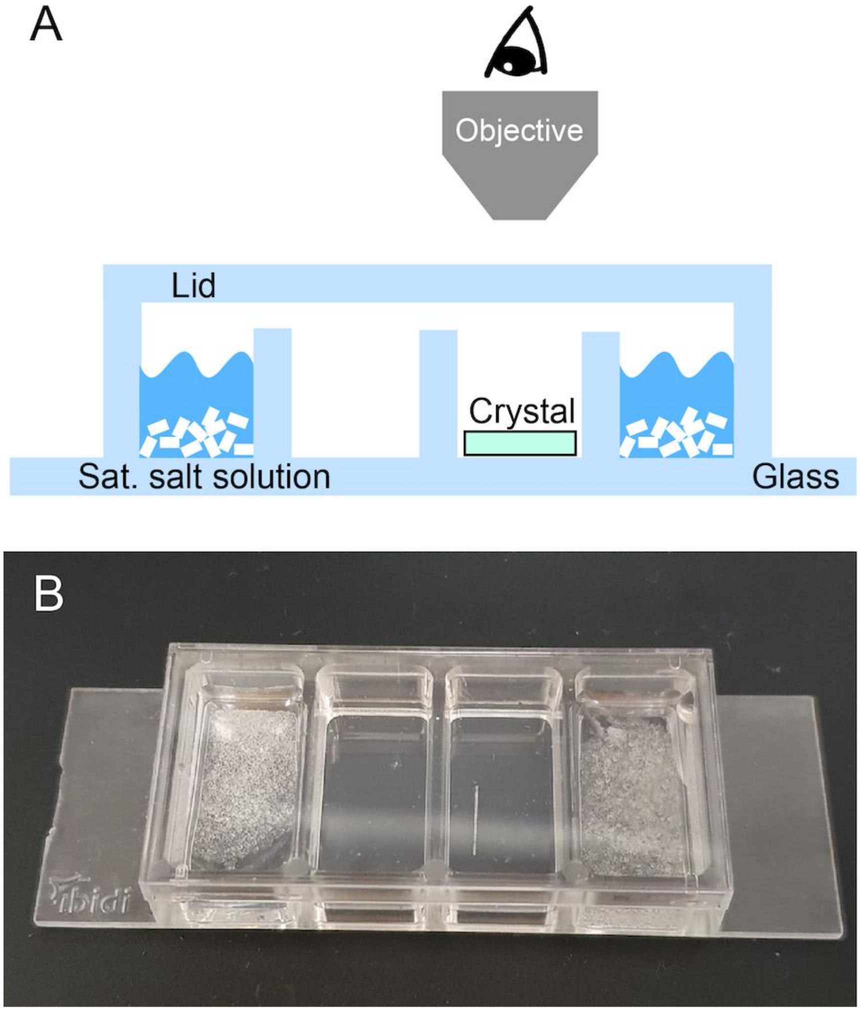

Supplementary Fig. 9. Apparatus used to perform controlled humidity experiments. (A) A schematic of the humidity-controlled experimental setup. (B) An image of the 4-well plate that contained saturated salt solutions used to maintain a constant humidity. A crystal of HCB was placed in the 3rd well from the left. The wells in this image contain a saturated NaCl solution of water. Similar experiments were performed by using solutions of other salts.

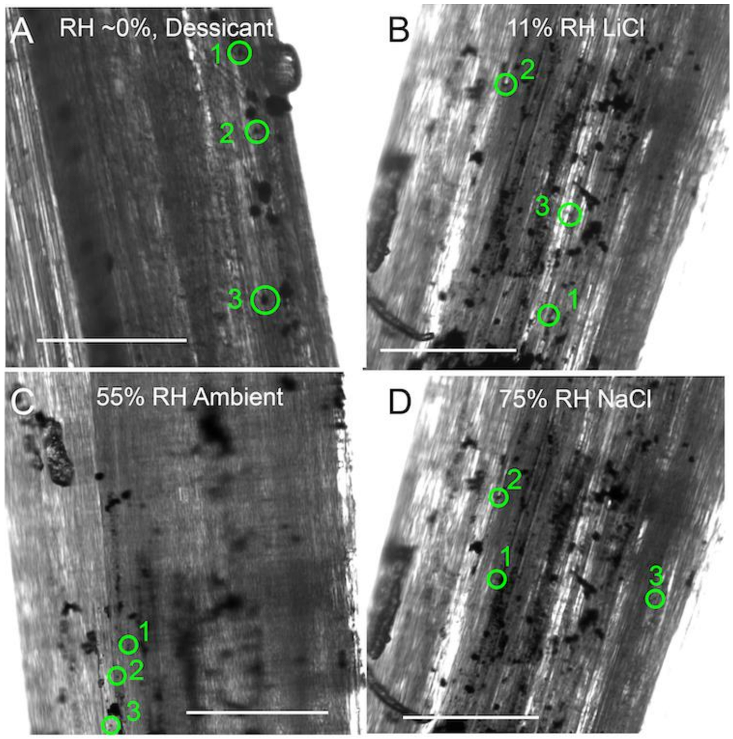

Supplementary Fig. 10. Greyscale image of the particle that were tracked under various relative humidity (RH) levels. The particles in the dessicated environment (A) were stationary and the particles in LiCl, ambient and NaCl (B, C and D,respectively) moved at consistant rates which confirmed that water necessary for motion . The AgMP in humidities above 55% moved faster than the AgMP in humidities below 55% which suggests that condensation on the surface of HCB happens more readily at RH's above 55% The contrast in these images has been enhanced to enable better particle tracking. All scale bars = 100 μm.

Supplementary Fig. 11. Confocal microscopy image of a AgMP being pulled during desiccation. Panels A–C show the surface of HCB while being desiccated at time points 1340, 1740, 2000 min for panels A, B and C, respectively. A particle is being *pulled* by a receding water meniscus. The blue arrow indicates the meniscus and the red circle shows the particle being pulled.

Supplementary Fig. 12. Confocal microscopy image of a AgMP being pushed with exposure to humidity. Panels A–C show the surface of HCB after it has been desiccated for 48 h and then exposed to 44% RH. A particle is being *pushed* by an expanding water meniscus. Panels A, B and C are at time points 100, 300 and 850 min. A blue arrow indicates the meniscus and the red circle shows the particle being pushed.

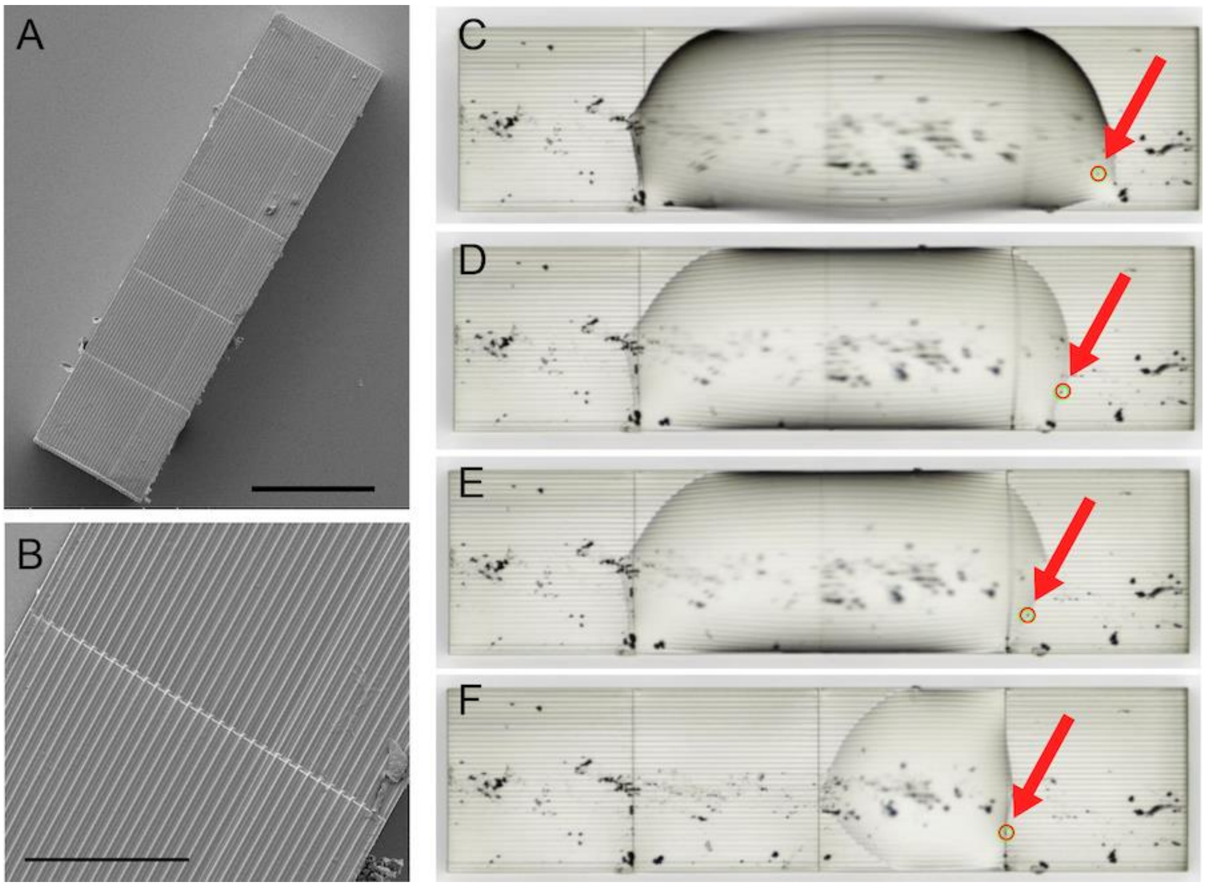

Supplementary Fig. 13. SEM and optical images of a 3D printed object with linear, static channels. (A) Scanning electron micrograph of the manufactured resin block and a zoom in on the channels. Scale bar = 250 μm. (B). Time lapse images of an AgMP aggregate moving as water recedes from the channel and pulls a AgMP along with the receding miniscus. Scale bar = 100 μm. (C–F) Optical images of the water receding on the resin block after 0, 43, 51, and 90 seconds. The manufactured resin block is 250 μm wide and 1 mm long.

Supplementary Tables

Supplementary Table 1. Distance, rate and size of seven AgMPs that were tracked at room temperature (21 °C) and 55% relative humidity

Particle #	Total distance (μm)	Average velocity (μm / h)	Velocity range (μm / h)	Velocity median (μm / h)	AgMP aggregate size (μm^2)	AgMP aggregate direction
1	8.6	2.29	1.17–3.48	2.32	4.88	Lower left
2	35.6	2.86	2.03–4.69	2.56	2.53	Lower left
3	33.6	2.68	1.93–3.25	2.78	3.14	Lower left
4	31.3	2.50	1.16–4.05	2.09	3.53	Lower left
5	25.9	2.07	1.48–2.48	2.09	3.44	Lower left
6	27.8	2.23	1.48–3.41	2.10	2.80	Lower left
7	13.8	1.15	0.0–1.93	1.16	70.89	Upper right

Supplementary Table 2. Dynamic contact angle measurements acquired using a tensiometer

Repetition #	Advancing contact angle (º)	Receding contact angle (º)
1	99.7	86.1
2	95.7	84.6
3	96.1	84.4
4	97.2	85.1
Average	97.2	85.1
STD deviation	1.8	0.8

Supplementary Table 3. Distance, rate and size of seven AgMPs that were tracked at 22.2–22.9 ºC and 44% relative humidity

Particle #	Total distance (μm)	Average velocity (μm / h)	Velocity range (μm / h)	Velocity median (μm / h)	AgMP aggregate size (μm^2)	AgMP aggregate direction
a	16.004	0.7	0.23–1.03	0.702	2.484	Down
b	25.966	1.12	0.70–1.26	1.17	13.35	Down
c	11.752	0.5	0.23–1.17	0.468	5.28	Down
d	20.154	0.86	0.47–1.17	0.702	1.4	Down
e	5.91	0.27	0.23–0.70	0.234	3.88	Down
f	8.043	0.38	0.23–0.70	0.336	1.86	Up
g	6.304	0.298	0.00–.468	0.234	4.97	Up

Supplementary Table 4. Distance, rate and size of seven AgMPs that were tracked at 27.9–36.0 ºC and 44% relative humidity

Particle #	Total distance (μm)	Average velocity (μm / h)	Velocity range (μm / h)	Velocity median (μm / h)	AgMP aggregate size (μm^2)	AgMP aggregate direction
h	13.64	0.91	0.31–1.63	0.94	5.41	Down
i	15.00	1.00	0.62–1.68	0.94	8.32	Down
j	20.31	1.35	0.94–1.94	1.25	3.51	Down
k	18.93	1.26	0.94–1.87	1.25	4.05	Down
l	25.94	1.73	1.25–1.96	1.87	1.62	Down
m	12.91	0.86	0.62-1.22	0.62	10	Down
n	8.01	0.85	0.62-1.37	0.94	8.11	Down

Supplementary Table 5. Distance, rate and size of seven AgMPs that were tracked at 31.3–40.5 ºC and 44% relative humidity

Particle #	Total distance (μm)	Average velocity (μm / h)	Velocity range (μm / h)	Velocity median (μm / h)	AgMP aggregate size (μm^2)	AgMP aggregate direction
o	30.2	1.42	1.80–10.32	3.35	9.73	Down
p	21.8	1.02	1.54–4.64	2.32	9.46	Down
q	23.7	1.11	0.36–6.30	2.20	4.36	Down
r	30.1	1.45	0.26–6.78	2.19	8.11	Down
s	36.2	2.38	1.16–12.12	5.67	6.49	Down
t	45.9	3.10	1.29–5.93	3.35	2.13	Down
u	57.4	2.69	0.77–7.22	2.06	2.43	Down

Supplementary Table 6. Distance, rate and size of seven AgMPs that were tracked at 36.0–41.0 ºC and 44% relative humidity

Particle #	Total distance (μm)	Average velocity (μm / h)	Velocity range (μm / h)	Velocity median (μm / h)	AgMP aggregate size (μm^2)	AgMP aggregate direction
v	28.66	2.15	1.44–3.28	1.92	5.13	Left
w	46.97	2.56	1.44–4.43	2.598	4.49	Left
x	74.99	3.21	1.44–6.24	2.4	3.21	Left
y	43.06	1.85	0.96–3.84	1.44	5.77	Left
z	27.58	1.82	0.96–4.03	1.68	9.6	Right
aa	54.03	6.23	4.63–8.81	5.052	3.8	Left
ab	30.92	2.18	0.96–3.36	2.316	1.92	Right

Supplementary Table 7. Distance, rate and size of seven AgMPs that were tracked at 34.7–41.5 ºC and 55% relative humidity

Particle #	Total distance (μm)	Average velocity (μm / h)	Velocity range (μm / h)	Velocity median (μm / h)	AgMP aggregate size (μm^2)	AgMP aggregate direction
8	54.9	4.11	1.80–10.32	3.35	1.86	Right, then left
9	13.4	2.75	1.54–4.64	2.32	6.01	Right
10	52.6	3.28	0.36–6.30	2.20	1.38	Left, then right
11	48.5	3.49	0.26–6.78	2.19	3.89	Left, then right
12	42.0	5.70	1.16–12.12	5.67	9.40	Right, then left
13	25.2	3.35	1.29–5.93	3.35	197.66	Right
14	38.3	2.65	0.77–7.22	2.06	2.32	Right

Supplementary Table 8. Velocity of three different AgMPs that were tracked at several relative humidity (RH) levels

Velocity (μm h^{-1})				
Particle #	1	2	3	Average
Desiccant (~0% RH)	0	0	0	0
LiCl (11% RH)	0.80	0.90	1.19	0.96
CH_3COOK (22% RH)	.71	1.02	.82	0.85
Ambient (55% RH)	1.54	2.27	1.48	1.76
NaCl (75% RH)	1.94	1.44	1.36	1.58